

Large-eddy simulation of heat transfer downstream of a backward-facing step

A Keating^{1,4}, U Piomelli², K Bremhorst¹ and S Nešić³

¹ Division of Mechanical Engineering, The University of Queensland, St. Lucia, QLD 4072, Australia

² Department of Mechanical Engineering, University of Maryland, College Park, MD 20910, USA

³ Institute for Corrosion and Multiphase Technology, Ohio University, Athens, OH 45701, USA

E-mail: akeating@eng.umd.edu

Received 6 February 2004

Published 17 May 2004

DOI: 10.1088/1468-5248/5/1/020

Abstract. Large-eddy simulation is used to predict heat transfer in the separated and reattached flow regions downstream of a backward-facing step. Simulations were carried out at a Reynolds number of 28 000 (based on the step height and the upstream centreline velocity) with a channel expansion ratio of 1.25. The Prandtl number was 0.71. Two subgrid-scale models were tested, namely the dynamic eddy-viscosity, eddy-diffusivity model and the dynamic mixed model. Both models showed good overall agreement with available experimental data. The simulations indicated that the peak in heat-transfer coefficient occurs slightly upstream of the mean reattachment location, in agreement with experimental data. The results of these simulations have been analysed to discover the mechanisms that cause this phenomenon. The peak in heat-transfer coefficient shows a direct correlation with the peak in wall shear-stress fluctuations. It is conjectured that the peak in these fluctuations is caused by an impingement mechanism, in which large eddies, originating in the shear layer, impact the wall just upstream of the mean reattachment location. These eddies cause a ‘downwash’, which increases the local heat-transfer coefficient by bringing cold fluid from above the shear layer towards the wall.

PACS numbers: 47.27.Eq, 47.27.Nz, 47.27.Te, 47.32.Ff

⁴ Present address: Department of Mechanical Engineering, University of Maryland, College Park, MD 20910, USA.

Contents

Nomenclature	2
1 Introduction	3
2 Numerical method	4
3 Computational details	5
4 Results and discussion	6
4.1 Mean reattachment length and coefficient of friction	6
4.2 Stanton number	14
4.3 Mean velocity and temperature fields	15
4.4 Streamwise velocity fluctuations and temperature variance	15
4.5 Turbulent heat fluxes	17
4.6 Mechanisms driving heat transfer in the recirculation zone	19
5 Conclusions	21
Acknowledgments	26
References	26

Nomenclature

C_{ev}	subgrid-scale eddy-viscosity coefficient
C_f	coefficient of friction
C_p	specific heat
C_θ	subgrid-scale eddy-diffusivity coefficient
h	step height
p	pressure
Pr	Prandtl number
q	heat flux
q_w	wall heat flux
Re	Reynolds number
S_{ij}	strain rate tensor
St	Stanton number
t	time
T	temperature
u_i	general notation for velocity components, $u_1 = u$, $u_2 = v$ and $u_3 = w$
U_c	upstream mean centreline velocity
x_i	general notation for spatial coordinates, $x_1 = x$, $x_2 = y$ and $x_3 = z$
δ_{ij}	Kronecker delta
Δ	filter width
ρ	density
τ	shear stress
$\langle \cdot \rangle$	fluctuation from the mean
$\bar{\cdot}$	grid filtered variable
$\langle \cdot \rangle$	time- and ensemble-averaged mean

1. Introduction

The separation and reattachment of turbulent flows are common features in engineering devices. They occur in many components of turbines, diffusers and combustors, as well as in external flows, including flows around buildings and aircraft. When heat transfer is involved, separation and reattachment cause large variations in the heat-transfer coefficient, and significant increases in heat transfer rates [1]. Reynolds-averaged turbulence modelling (without significant tuning of the models) has been found to be generally incapable of an accurate prediction of the fluid dynamics and heat transfer in these types of flow [2], of which the backward-facing step is a well-studied, simplified example.

Reviews of early experimental heat transfer studies in separating and reattaching flows can be found in [3]–[5]. Kottke [6] formulated an empirically derived formula for the maximum heat transfer from (or to) the wall. By far the most comprehensive experimental study is that of Vogel and Eaton [1], who performed a combined study of fluid dynamics (using laser-Doppler anemometry, LDA) and heat transfer (using thermocouple probes). The Reynolds number in their experiments was 28 000, and the channel had an expansion ratio of 1.25 (the ratio of the downstream channel height to the upstream channel height). In the experiments, Vogel and Eaton [1] found that the maximum heat transfer occurred at approximately 2/3 of a step-height upstream of the mean reattachment location. They found that, while the heat-transfer coefficient did not show a good correlation with the time-averaged skin-friction coefficient (i.e. through the Reynolds analogy of heat and momentum transfer), it showed remarkable agreement with the fluctuations of the skin friction coefficient.

Large-eddy simulations of heat transfer, downstream of a backward-facing step, have been recently published by Avancha and Pletcher [7] and Labbe *et al* [8]. Avancha and Pletcher's simulation [7] concentrated on flows in which the heat transfer caused significant property variations. They used a coupled, compressible, finite-volume code with a dynamic eddy-viscosity/eddy-diffusivity subgrid-scale model. The Reynolds number was 5540 and the expansion ratio was 1.5. The results showed reasonable agreement with the particle-tracking velocimetry (PTV) experimental data of Kasagi and Matsunaga [9]; it is probable that the discrepancies observed were caused by the coarse grid used. Due to the low Reynolds number simulated, no direct comparisons of the heat transfer field with experimental results could be made. However, good qualitative agreement with the Vogel and Eaton [1] experiments was found. As in the experiments, the LES of Avancha and Pletcher [7] also indicated that the peak in heat-transfer coefficient occurred just upstream of the mean reattachment location. Their simulations showed the wall heat-transfer coefficient had the same behaviour as the fluctuating skin-friction coefficient, and was also correlated with the thickness of the viscous sublayer.

Labbe *et al* [8] used a mixed scale subgrid-scale model with a constant subgrid-scale Prandtl number to perform an LES of heat transfer downstream of a backward-facing step. The Reynolds number was 7432 and the step had an expansion ratio of 1.1. They validated their LES simulations by comparing the mean reattachment length to experimental data. In contrast with both the experimental data of Vogel and Eaton [1] and the LES of Avancha and Pletcher [7], Labbe *et al* [8] found that maximum heat transfer occurred at the point of reattachment. It is unclear why this occurred in these simulations and it is especially difficult to make conclusions due to the lack of available experimental results for comparison.

The present simulation aims to resolve two issues. First, large-eddy simulation are carried out at a Reynolds number high enough to allow for direct comparison with experimental data. Second, the results of these simulations are used to investigate the mechanisms involved in heat transfer to and from the wall in the recirculation and reattachment zones.

2. Numerical method

The equations governing fluid flow and heat transfer of an incompressible fluid solver for large-eddy simulation are obtained by applying a filtering operation to the Navier–Stokes, continuity and temperature equations, which results in

$$\frac{\partial \bar{u}_i}{\partial x_i} = 0, \quad (1)$$

$$\frac{\partial \bar{u}_i}{\partial t} + \frac{\partial \bar{u}_j \bar{u}_i}{\partial x_j} = \frac{1}{Re} \frac{\partial^2 \bar{u}_i}{\partial x_j \partial x_j} - \frac{\partial \bar{p}}{\partial x_i} - \frac{\partial \tau_{ij}}{\partial x_j}, \quad (2)$$

$$\frac{\partial \bar{T}}{\partial t} + \frac{\partial \bar{T} \bar{u}_j}{\partial x_j} = \frac{1}{Re \cdot Pr} \frac{\partial^2 \bar{T}}{\partial x_j \partial x_j} - \frac{\partial q_j}{\partial x_j}, \quad (3)$$

where overbars indicate filtered quantities. The above equations have been normalized by the upstream mean centreline velocity, U_c , and step height, h , resulting in $Re = hU_c/\nu$ and $Pr = \nu/\alpha$, where ν is the kinematic viscosity and α the molecular diffusivity. Note that buoyancy and other variable property effects have been neglected. The subgrid-scale stress term, τ_{ij} , and the subgrid-scale heat flux term, q_j , contain the effects of the subgrid scales on the resolve scales:

$$\tau_{ij} = \bar{u}_i \bar{u}_j - \bar{u}_i \bar{u}_j, \quad (4)$$

$$q_j = \bar{T} \bar{u}_j - \bar{T} \bar{u}_j. \quad (5)$$

These terms contain quantities that cannot be obtained from the resolved velocity and temperature fields, and therefore must be modelled. Two subgrid-scale models were used here, the first is the dynamic eddy-viscosity/eddy-diffusivity model:

$$\tau_{ij} - \frac{\delta_{ij}}{3} \tau_{kk} = -2C_{ev} \bar{\Delta}^2 |\bar{S}| \bar{S}_{ij}, \quad (6)$$

$$q_j = -C_\theta \bar{\Delta}^2 |\bar{S}| \frac{\partial \bar{T}}{\partial x_j}, \quad (7)$$

where C_{ev} and C_θ are calculated using the dynamical procedure [10] and averaged over Lagrangian fluid pathlines [11].

The second subgrid-scale model used was the dynamical mixed model, in which a scale-similar term has been added to the eddy-viscosity and eddy-diffusivity terms:

$$\tau_{ij} = \bar{u}_i \bar{u}_j - \bar{u}_i \bar{u}_j - 2C_{ev} \bar{\Delta}^2 |\bar{S}| \bar{S}_{ij}, \quad (8)$$

$$q_j = \bar{T} \bar{u}_j - \bar{T} \bar{u}_j - C_\theta \bar{\Delta}^2 |\bar{S}| \frac{\partial \bar{T}}{\partial x_j}. \quad (9)$$

As in the dynamic eddy-viscosity, eddy-diffusivity model, C_{ev} and C_θ have been calculated using the dynamical procedure [10]. Here the mathematically consistent form [12] of the scale-similar terms was used in the dynamic procedure. The coefficients were again averaged over Lagrangian fluid pathlines [11].

The Navier–Stokes equations were spatially discretized using second-order finite differences on a staggered grid. The temperature equation was discretized using second-order finite

LES of heat transfer downstream of a BFS

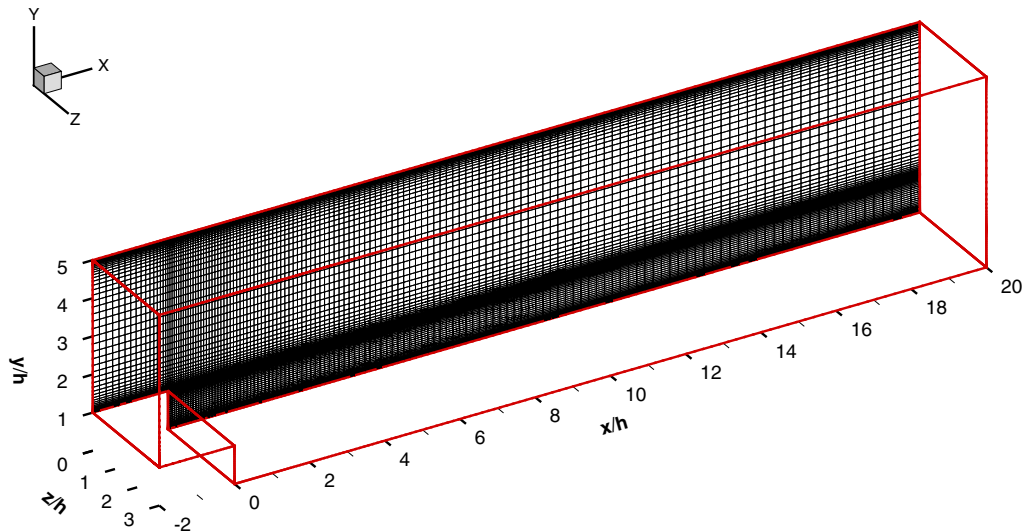


Figure 1. Computational geometry with computational grid.

differences for the diffusive terms and quadratic upstream interpolation (QUICK) for the convective terms [14]. QUICK was used to reduce the oscillations which are especially significant in the temperature equation when inflow–outflow boundary conditions (rather than periodic) are used [13]. Due to their damping effect on the turbulent spectra, upwind schemes are generally seen to be unsuitable for LES and DNS [15]. However, in the case of heat transport, this damping is relatively minor, as the lack of scale interaction implies that the damping of the small scales does not affect the large scales [16].

The equations were integrated in time using a fractional step method [17]. All terms except the wall-normal convective and diffusive terms were advanced explicitly in time using a third-order Runge–Kutta method. The wall-normal convective and diffusive terms were advanced implicitly using a second-order Crank–Nicolson method to remove the stability limits imposed by grid refinement near the walls and at the step edge. Because of the implicit treatment of the wall-normal convective term, the wall-normal momentum equation becomes non-linear. A Taylor series expansion of the wall-normal convective term was performed to linearize this equation [13].

The additional cross-derivative terms that arise in the eddy-viscosity subgrid-scale model were advanced explicitly in time using the third-order Runge–Kutta method. Spatial discretization of the scale-similar terms in the mixed model was performed using the same methods as those used for the convective terms in the momentum and temperature equations. Test and grid filtering (the latter for the dynamical mixed model only) was performed in all three directions using trapezoidal rule filters of widths $\sqrt{6}$ and $\sqrt{3}$ respectively.

3. Computational details

The simulation was carried out in the same configuration as the experiments of Vogel and Eaton [1]. Further data on these experiments are presented in [22] and in [23]. A schematic layout of the simulation domain is shown in figure 1. The channel expansion ratio was 1.25, with a Reynolds number of 28 000 (based on the freestream velocity and step height, h). The experiment was carried out with an inflow condition consisting of two developing boundary layers separated by a relatively undisturbed core. These boundary layers had a measured thickness

Table 1. Mean reattachment lengths.

	x/h	Deviation from experiment [23]
Experiment [23]	6.7 ± 0.1	
LES [19]	6.74	0.6%
Present, LES, dynamic eddy-viscosity model	6.54	2.5%
Present, LES, dynamic mixed model	6.60	1.5%

of $\delta/h = 1.1$. Heat transfer measurements were made in air with a Prandtl number of 0.71. On the lower wall, the heat flux was 270 W m^{-2} . All other walls were insulated. Variable property effects were minimized by having a maximum overheat of 15°C . The total domain size used for the computations was $22h \times 5h \times 3h$, which included an entry length of $2h$. A grid containing $144 \times 96 \times 96$ nodes was used, which was stretched in the wall-normal and streamwise directions using hyperbolic tangent functions to cluster grid points at the step edge and in the wall boundary layers. The grid stretching can be observed in figure 1. Results were also obtained on a finer grid containing $192 \times 128 \times 128$ nodes using the dyamic eddy-viscosity model (due to its lower computational cost).

Due to the need to supply a time-varying turbulent inflow condition, a time-series obtained from a separate periodic channel flow simulation was used at the inflow plane. A forcing method [16] was used to force the periodic channel flow simulation to match the experimental results for the mean and fluctuations of streamwise velocity. A convective boundary condition [18] was used at the exit plane. A constant heat flux boundary condition for the temperature field (non-dimensionalized in the simulation as $T^* = T/T_{ref}$) was applied along the lower wall and was non-dimensionalized as

$$q_w^* = \frac{q_w}{\rho C_p U_c T_{ref}}, \quad (10)$$

where q_w is the heat flux applied experimentally (270 W m^{-2}). The following properties of air at 293 K and 1 atm were used: $\rho = 1.205 \text{ kg m}^{-3}$, $C_p = 1005 \text{ J kg}^{-1} \text{ K}^{-1}$ and $Pr = 0.71$. The heat flux on all then other walls was set to zero. The inflow temperature was set constant at T_{ref} . A convective outflow boundary condition was used for the temperature at the outflow.

A constant CFL number of 1.0 was used to determine the computational timestep. Statistics were averaged in the homogeneous spanwise direction and over 100 (for the $144 \times 96 \times 96$ grid) or 50 (for the finer grid) realizations of the flow field. Each realization was separated by five non-dimensional time units, which corresponds to an overall averaging time of around 22 flow-through times (for the $144 \times 96 \times 96$ grid) or 10 flow-through times (for the finer grid).

4. Results and discussion

4.1. Mean reattachment length and coefficient of friction

The time-averaged mean reattachment length was computed from the coefficient of friction on the lower wall. Table 1 summarizes the reattachment lengths obtained for the two $144 \times 96 \times 96$ grid simulations presented here, the simulation of Akselvoll and Moin [19] and the experimental data. The present results using the dynamic mixed model and the results obtained by Akselvoll and Moin [19] are within the estimated experimental error bounds, while the results obtained using the dynamic eddy-viscosity model are just outside these bounds.

LES of heat transfer downstream of a BFS

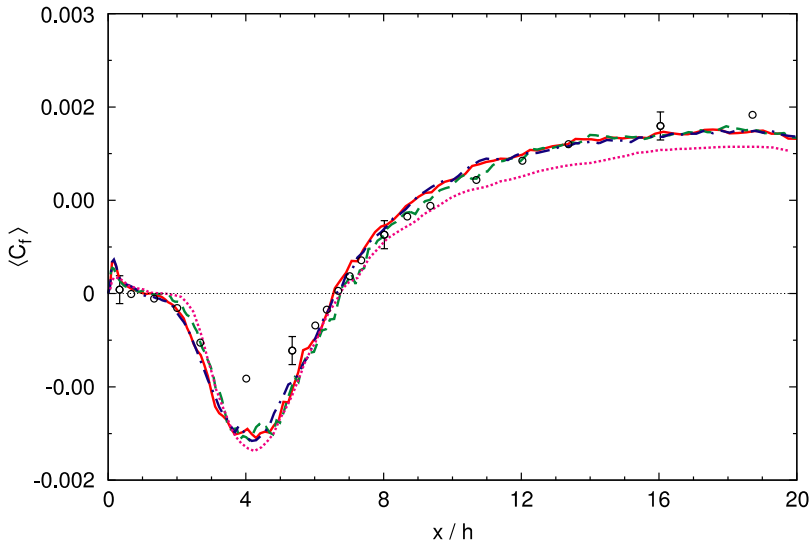


Figure 2. Coefficient of friction along the lower wall. —, LES, dynamic eddy-viscosity model, $144 \times 96 \times 96$; - - -, LES, dynamic eddy-viscosity model, $192 \times 128 \times 128$; — · —, LES, dynamic mixed model, $144 \times 96 \times 96$; · · · · ·, LES, Akselvoll and Moin [19]; ○, Adams *et al* [23].

The coefficient of friction is defined as

$$C_f = \frac{\tau_w}{\frac{1}{2}\rho U_c^2}, \quad (11)$$

where τ_w is the shear stress at the wall and U_c is the inlet velocity. The computed coefficient of friction along the lower wall is compared to the experimental results in figure 2. There are no known differences between the subgrid-scale models. The results show a similar agreement with the experimental results as the simulations by Akselvoll and Moin [19]: good agreement upstream of $x/h = 2$ and from reattachment to $x/h = 16$, but poor agreement in both the recirculation zone and downstream of $x/h = 16$. The reason for the poor agreement downstream of $x/h = 16$ is probably the effect of the outflow boundary condition. In the recirculation zone, it is unclear why all the LES simulations predict a larger negative value of C_f . Akselvoll and Moin [19] noted that this could be caused by either the inflow generation method used or by inadequate grid resolution in this region. Results obtained using the finer grid are also shown in figure 2 and indicate that the agreement with the experimental results is not improved with grid refinement. Another cause could be the limited spanwise extent of the domain; however, some preliminary simulations in wider domains did not result in improved results.

Figure 3 shows the rms of the friction coefficient fluctuations in the streamwise direction. The friction coefficient fluctuations predicted by the dynamic mixed model are lower than those predicted by the dynamic eddy-viscosity model. The peak in the friction coefficient fluctuations occurs between one- and two-step heights upstream of the mean reattachment point. Both subgrid-scale models show reasonable agreement with the experimental data and grid refinement does not seem to affect the results. The location of the peak in the LES results is shifted upstream of the experimental results, although it remains within the experimental error bounds. The rms of the spanwise component of the friction coefficient fluctuations is shown in figure 4. Again both models show similar trends, with the dynamic mixed model results lying slightly below the dynamic eddy-viscosity results.

In the recirculation zone, the fluctuations in the coefficient of friction are of the same order of magnitude as the time-averaged mean C_f . Using DNS results, Jeon *et al* [20] calculated the

LES of heat transfer downstream of a BFS

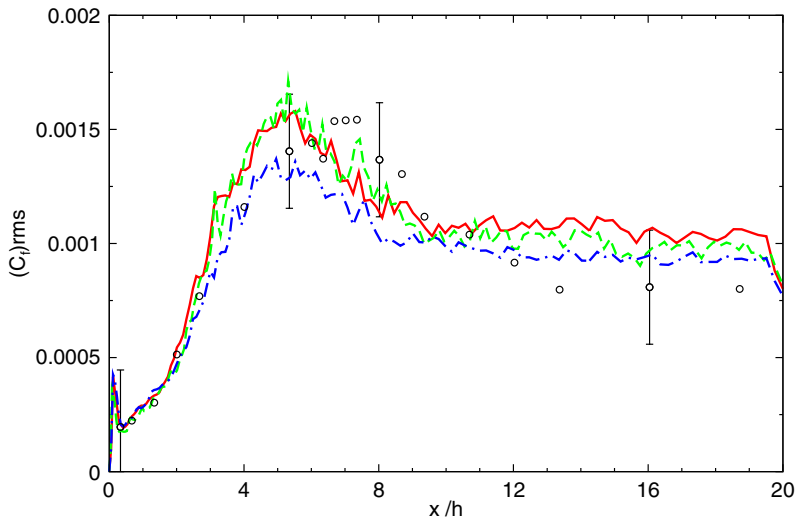


Figure 3. Rms of the coefficient of friction fluctuations (streamwise component) along the lower wall. —, LES, dynamic eddy-viscosity model, $144 \times 96 \times 96$; - - -, LES, dynamic eddy-viscosity model, $192 \times 128 \times 128$; — · —, LES, dynamic mixed model, $144 \times 96 \times 96$; ○, Vogel [22].

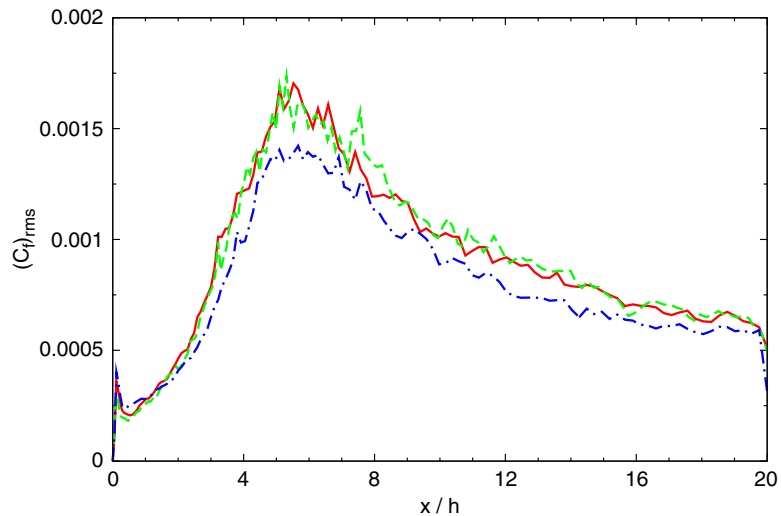


Figure 4. Rms of the coefficient of friction fluctuations (spanwise component) along the lower wall. —, LES, dynamic eddy-viscosity model, $144 \times 96 \times 96$; - - -, LES, dynamic eddy-viscosity model, $192 \times 128 \times 128$; — · —, LES, dynamic mixed model, $144 \times 96 \times 96$.

rms of the fluctuating shear stress components to be 36% (for the streamwise component) and 20% (for the spanwise component) of their means for turbulent channel flow. In the recirculation zone, the ratio of fluctuations in the coefficient of friction to its time-averaged mean was found to be around 75% for both components. This is significantly higher than reported for channel flow and is thought to be the result of shear-layer eddies impinging on the lower wall.

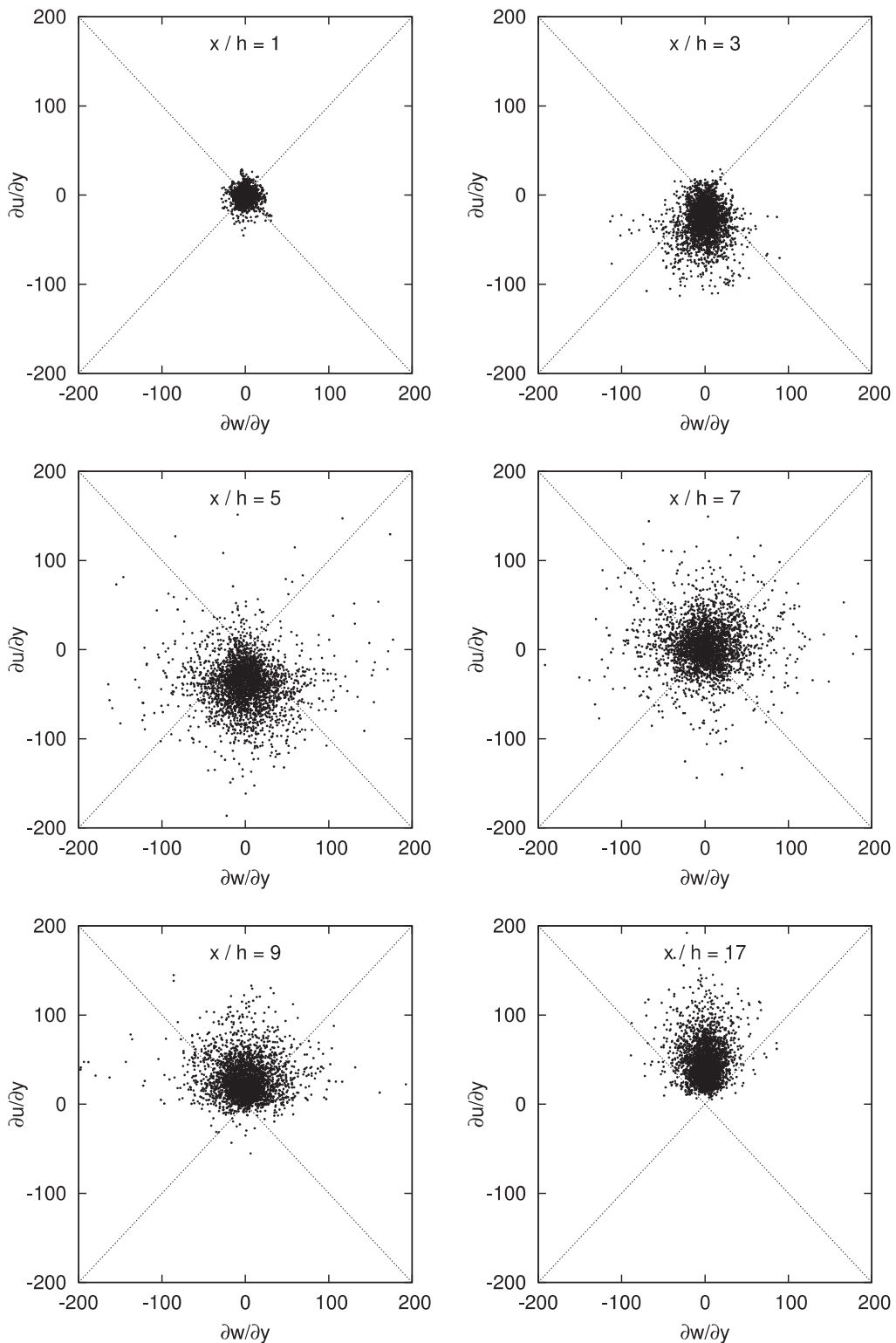
Downstream of the primary reattachment point, the shear-stress fluctuations decay as the boundary-layer develops and the impinging shear layer has less of an effect. The decay of the spanwise fluctuations is faster than that of the streamwise fluctuations; far downstream, the spanwise fluctuations are significantly lower than the streamwise ones. This difference in the rate of decay is probably caused by the fact that a combination of two different mechanisms causes streamwise wall shear-stress fluctuations, while only one of these mechanisms causes fluctuations in the spanwise direction. Studies of turbulent channel flow [20] indicate that the near-wall mean streamwise motion in boundary-layer flows (due to the near-wall streaks) primarily cause streamwise fluctuations, the spanwise ones being somewhat smaller in magnitude. This is shown in the relative magnitudes of the shear-stress fluctuations downstream of the reattachment location. However, near reattachment, the relative magnitudes of the shear-stress fluctuations are similar, which is the result of the impinging shear-layer eddies. Downstream of reattachment, therefore, the spanwise shear-stress fluctuations probably decay faster due to a reduction in the number of shear-layer eddies that impinge on the wall.

In a fully developed boundary layer, the near-wall streaks cause the instantaneous wall shear-stress vector to be primarily oriented in the mean flow direction. In turbulent channel flow, the instantaneous shear-stress vector was found to deviate rarely more than 45° from the mean flow direction [20]. Figure 5 shows scatter plots of the components of the wall shear stress vector components, $\partial u / \partial y$ and $\partial w / \partial y$. Two distinct behaviours are observed. Far downstream of the mean reattachment location, the results are similar to those for turbulent channel flow [20] with the wall shear stress vector primarily oriented in the direction of the mean flow, and rarely showing an angle greater than 45° away from that direction. This behaviour is also observed in the reversed-flow region. A different behaviour is observed near reattachment. In this region, the instantaneous wall shear-stress vectors have a significant spanwise component (which is of similar magnitude to the streamwise one). There are two possible reasons for this behaviour: either shear-layer eddies impinging on the wall and being restricted by other motions in the streamwise direction (i.e. the recirculation bubble), cause momentum transfer in the spanwise direction; or the lack of a mean flow direction to stretch the near-wall structures in the streamwise direction.

Probability density functions (PDFs) of the components of the instantaneous wall shear stress are shown in figures 6 and 7. Gaussian PDFs with a mean and variance matching the simulation results are also shown (as dotted lines) for comparison. These PDFs reinforce the notion of two distinct behaviours of the instantaneous wall shear-stress. Downstream of reattachment and well inside the recirculation zone, the PDFs of $\partial u / \partial y$ show positive or negative (depending on the mean flow direction) skewness indicating asymmetry of the wall shear stress. As discussed previously, this asymmetry is caused by the near-wall streaks in fully-developed boundary layer flow. Near the reattachment point, the skewness in $\partial u / \partial y$ has disappeared. At all locations, the PDFs of $\partial w / \partial y$ show effectively zero skewness, i.e. they are not affected by the mean flow direction. This also confirms the two-dimensionality of the time-averaged flow. Near reattachment, both $\partial u / \partial y$ and $\partial w / \partial y$ show high levels of flatness (indicated by larger-than-Gaussian tails in the PDFs) which reveal the presence of infrequent events that are large in magnitude. This is a further indication that shear-layer eddies impinge the wall slightly upstream of the reattachment point.

Instantaneous shear-stress vectors along the lower wall are shown in figure 8. The significant spanwise component of the instantaneous wall shear-stress near reattachment is clearly evident near and just upstream of the mean reattachment point (contrast this to the instantaneous shear-stress vectors well downstream of reattachment, which are clearly oriented in the streamwise direction). Overlaid on the shear stress vectors are contours of near-wall, wall-normal velocity. This shows that high levels of near-wall towards-the-wall velocities are strongly correlated with

LES of heat transfer downstream of a BFS

**Figure 5.** Scatter plots of instantaneous wall shear stress.

LES of heat transfer downstream of a BFS

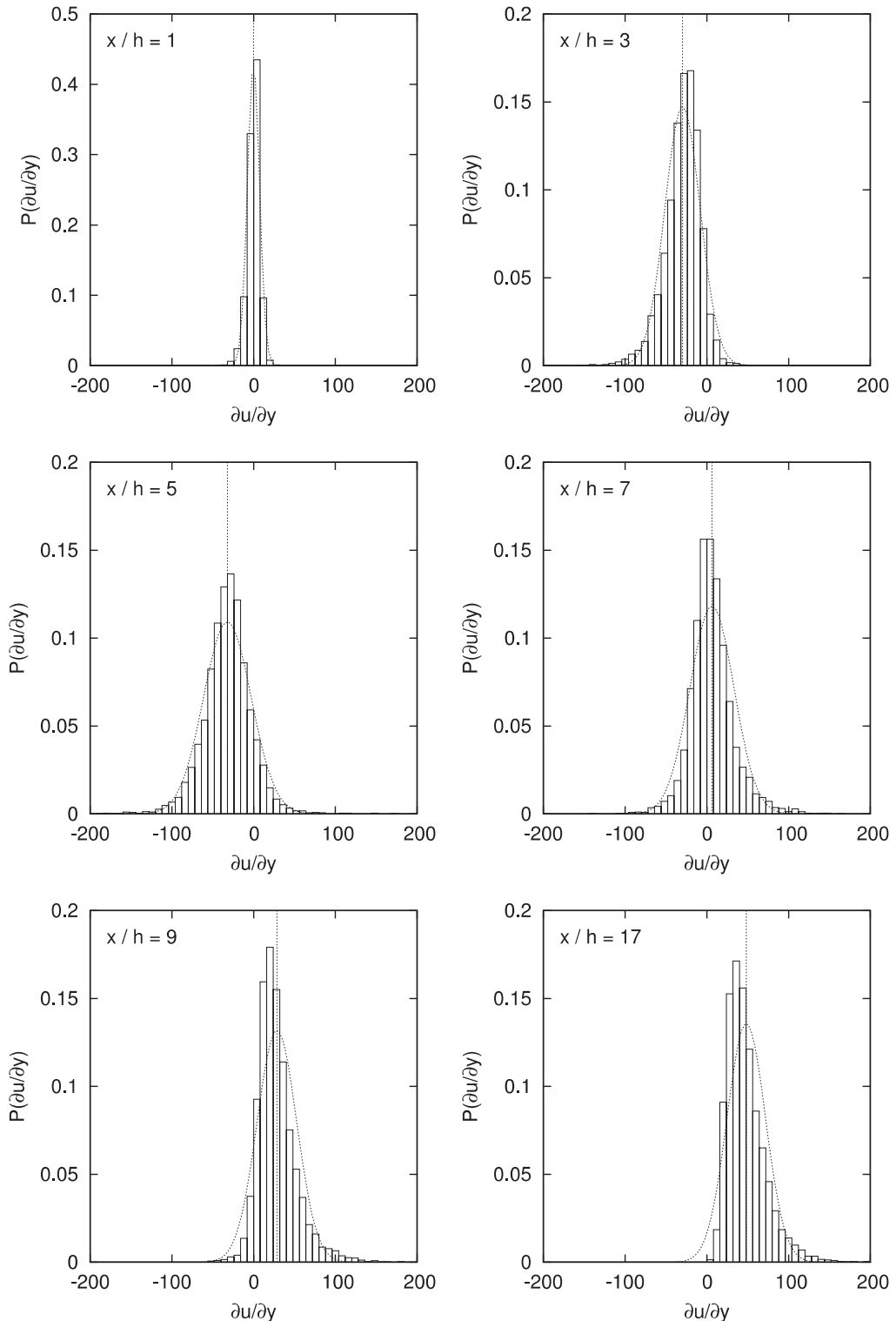


Figure 6. Probability distribution of $\partial u / \partial y$ at the lower wall. Dotted vertical line indicates mean. Dotted curve indicates a Gaussian distribution with the mean and variance of the distribution.

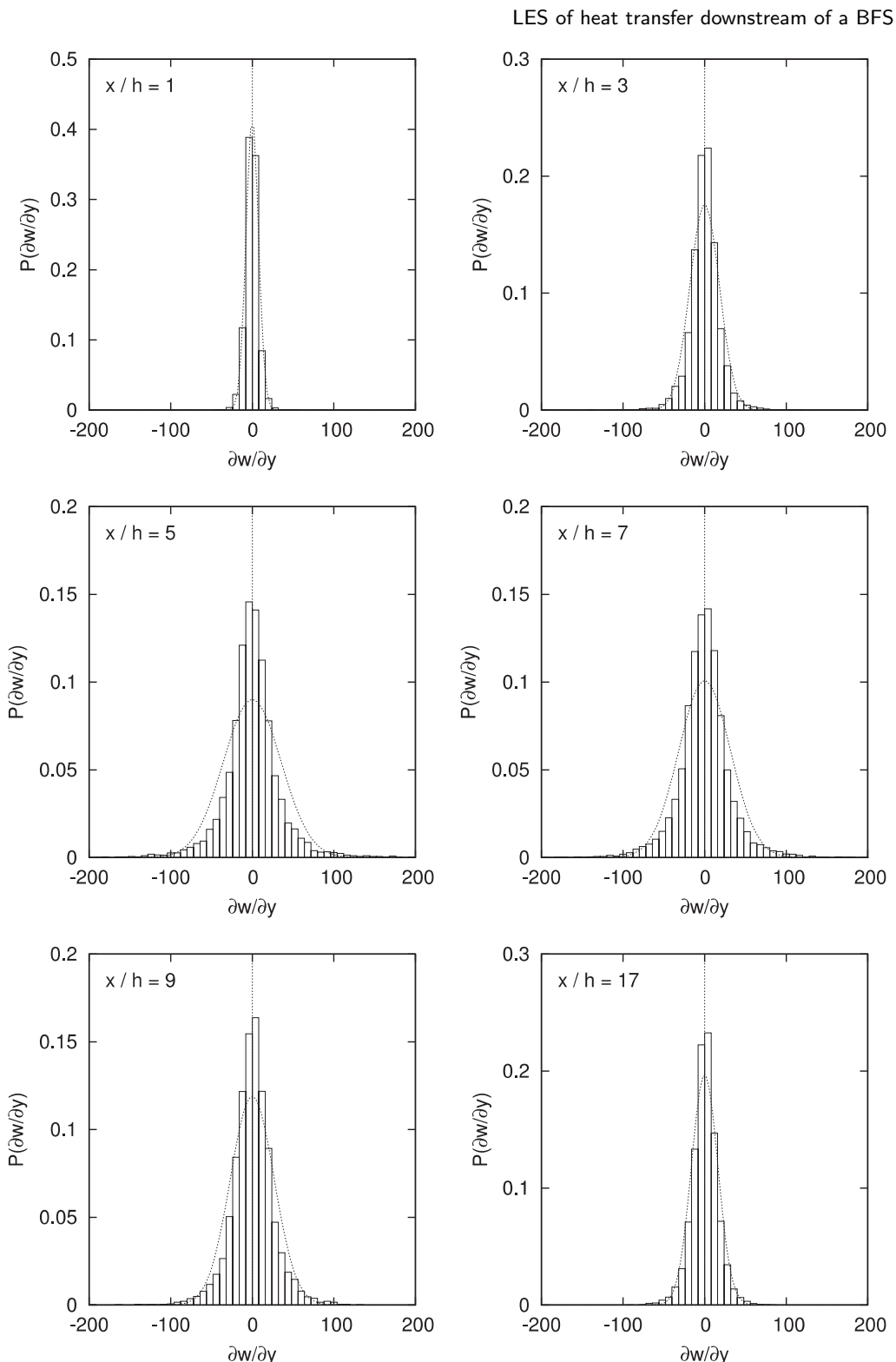


Figure 7. Probability distribution of $\partial w / \partial y$ at the lower wall. Dotted vertical line indicates mean. Dotted curve indicates a Gaussian distribution with the mean and variance of the distribution.

LES of heat transfer downstream of a BFS

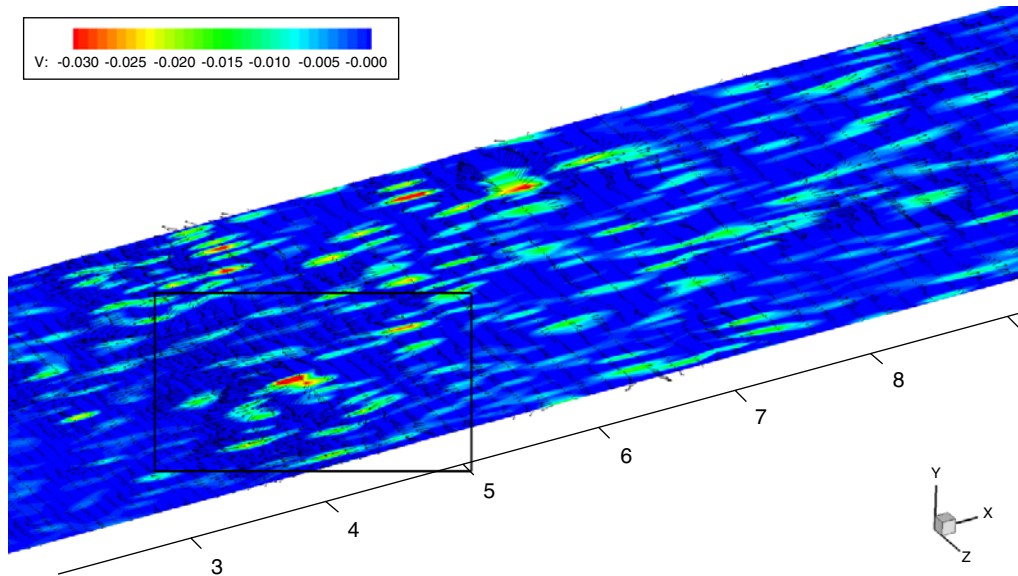


Figure 8. Visualization of near-wall, wall-normal velocity and wall shear stress vectors. Box indicates extent of figure 9.

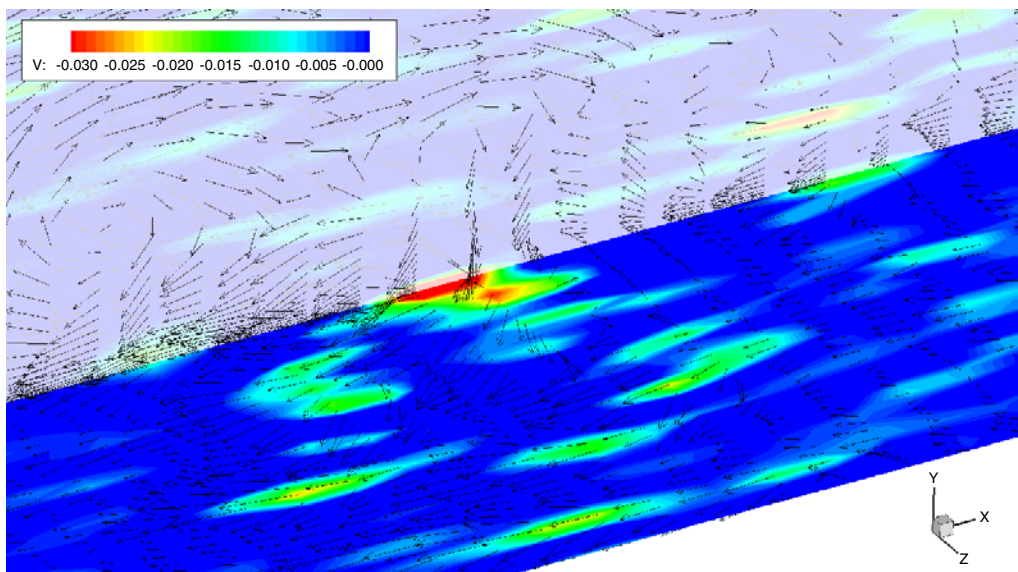


Figure 9. Visualization of a typical ‘downwash’ event. On the xz -horizontal plane are plotted contours of near-wall wall-normal velocity with tangential velocity vectors. On the vertical xy -plane (transparent) are tangential velocity vectors.

the upstream end of regions of high levels of instantaneous wall shear stress. This ‘downwash’ type event was also observed experimentally [21]. Kostas [21] proposed that these events were the result of ‘a structure whose physical size is such that an interaction with the wall is unavoidable.’ The size of these eddies also cause them to have a significantly high momentum. A visualization of a typical ‘downwash’ event is shown in figure 9. Here an eddy can be seen impacting the wall, causing a large towards-the-wall velocity event, resulting in a large fluctuation in wall shear stress.

LES of heat transfer downstream of a BFS

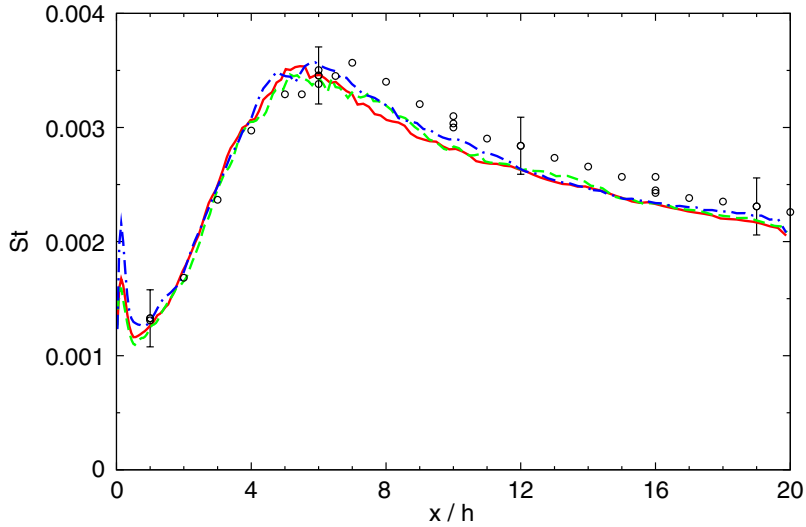


Figure 10. Stanton number along the lower wall. —, LES, dynamic eddy-viscosity model, $144 \times 96 \times 96$; - - -, LES, dynamic eddy-viscosity model, $192 \times 128 \times 128$; - · -, LES, dynamic mixed model, $144 \times 96 \times 96$; O, Vogel and Eaton [1].

4.2. Stanton number

In fully developed turbulent flow (such as in turbulent channel flow or flow over a flat plate), the Reynolds analogy is expected to be valid; namely, heat transfer between a surface and the fluid is directly related to the skin-friction coefficient

$$\frac{C_f}{2} = St. \quad (12)$$

The Stanton number, a non-dimensional measure of the heat transfer to or from the wall, is defined as

$$St = \frac{h}{\rho C_p U_c}, \quad (13)$$

where the heat-transfer coefficient h is

$$h = \frac{q_w}{T_w - T_{ref}}; \quad (14)$$

by using the non-dimensional form of the wall heat flux, q_w^* , and wall temperature, T_w^* , the Stanton number can be obtained from

$$St = \frac{q_w^*}{T_w^* - 1}. \quad (15)$$

However, the experiments of Vogel and Eaton [1] and the LES of Avancha and Pletcher [7] both indicate that Reynolds analogy does not hold in the recirculation zone. Figure 10 shows the Stanton number profile along the lower wall. No significant differences are observed between the coarse- and fine-grid results. Both subgrid-scale models produce similar results, with the biggest difference occurring next to the step edge, where the dynamic mixed model predicts a

larger amount of heat transfer from the wall. The other difference between the two subgrid-scale models is in the region between $x/h = 6$ and $x/h = 9$, where the dynamic mixed model produces slightly larger values of Stanton number. There is generally good agreement with the experimental results. The agreement with experimental results is better than that for the coefficient of friction, probably because of the different mechanisms that drive the heat and momentum transfer. As suggested earlier, a possible cause for the discrepancy in the skin friction coefficient was the spanwise extent of the domain. As will be shown, the heat transfer is driven by small-scale events that occur close to the surface, which are not likely to be affected by a short spanwise domain size. The peak in the computed profiles of St is slightly upstream of the peak in the measurements. This also causes the Stanton number to begin decaying earlier. From the plots of C_f along the lower wall (figure 2) and the Stanton number profile (figure 10), it is clear that Reynolds' analogy is not valid in the recirculation zone or near reattachment, where C_f vanishes but St is near its peak value. As in the experiments and the previous LES of Avancha and Pletcher [7], there is, however, a strong similarity between the shape of the Stanton number profiles and the rms of the skin-friction fluctuations. Both of these profiles show a peak approximately one step-height upstream of reattachment. Note that for both of these variables the LES results show a peak slightly further upstream than the experimental results. In this region there are large fluctuations in Stanton number and some of the scatter in the LES results may be due to statistical uncertainty.

4.3. Mean velocity and temperature fields

Figure 11 shows the mean streamwise velocity at a number of locations downstream of the step. The results of the two subgrid-scale models are virtually indistinguishable. The finer grid results show a slightly stronger reversed flow in the recirculation zone (figure 12). Both models show generally good agreement with the experimental results with the major differences occurring downstream of reattachment and in the recirculation region. Downstream of reattachment both subgrid-scale models show smaller velocities than the experiments. The LES results of Akselvoll and Moin [19] also showed velocities smaller than the experimental results in this region, which they attributed to the flow gaining momentum as it passes downstream (due to side-wall boundary-layer growth) in the experiments. The primary discrepancy with the experimental results is in the recirculation region (at $x/h = 3$ and 5), where both subgrid-scale models predict a stronger backflow, linked to the prediction of a larger coefficient of friction in this region.

Profiles of the mean temperature field are shown in figure 13, and are compared with the experimental measurements of Vogel and Eaton [1]. As in the experiments, significant gradients in temperature are only present very close to the lower wall. Results from the two subgrid-scale models are nearly identical, except at the location nearest to the step, $x/h = 0.33$. Here the temperatures predicted by the dynamic mixed model are lower than those obtained with the dynamic eddy-viscosity model, and seem to be in better agreement with the experimental measurements. Overall, the agreement of the simulations with the experiments is good. Again, the finer-grid results are identical to the coarse-grid results. Downstream of reattachment, the simulations show the temperature field diffusing slightly further from the wall than in the experiments. This could be caused by the increase in mass flow experienced in the experiments due to the side wall boundary layer growth.

4.4. Streamwise velocity fluctuations and temperature variance

Profiles of the rms of the resolved streamwise velocity fluctuations are shown in figure 14. Both subgrid-scale models give similar results. Overall, the agreement of the simulation results with

LES of heat transfer downstream of a BFS

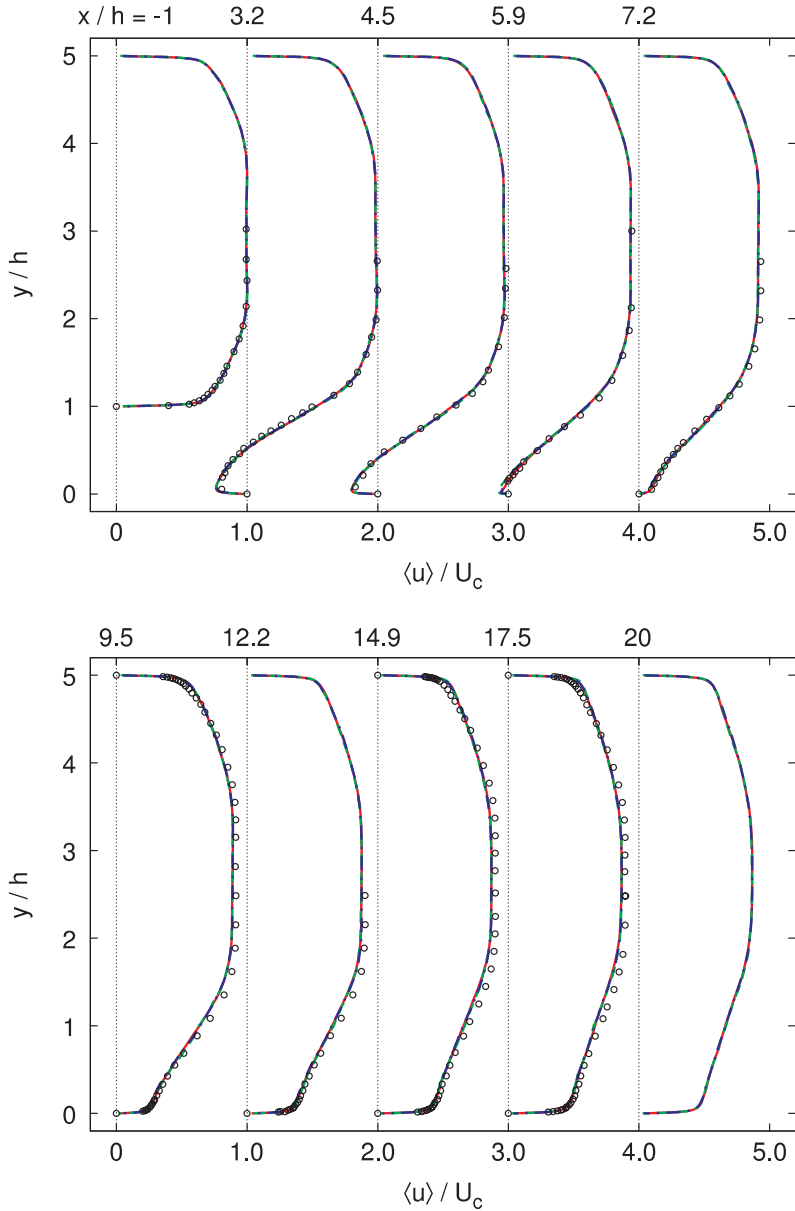


Figure 11. Mean streamwise velocity profiles: —, LES, dynamic eddy-viscosity model, $144 \times 96 \times 96$; - - -, LES, dynamic eddy-viscosity model, $192 \times 128 \times 128$; — · —, LES, dynamic mixed model, $144 \times 96 \times 96$; ○, Adams *et al* [23].

the measurements is good, especially considering that the subgrid-scale contribution of the eddy-viscosity term is not included (the scale-similar term is, however, included). Downstream of reattachment, there is some overprediction of the streamwise velocity fluctuations (especially near the upper wall), which is probably caused by insufficient grid resolution. The results obtained on the finer grid show, in general, a lower value of streamwise velocity fluctuations, especially near the walls.

Figure 15 shows profiles of the rms of the resolved temperature fluctuations. The differences between the two subgrid-scale models are again minimal, with the dynamic mixed

LES of heat transfer downstream of a BFS

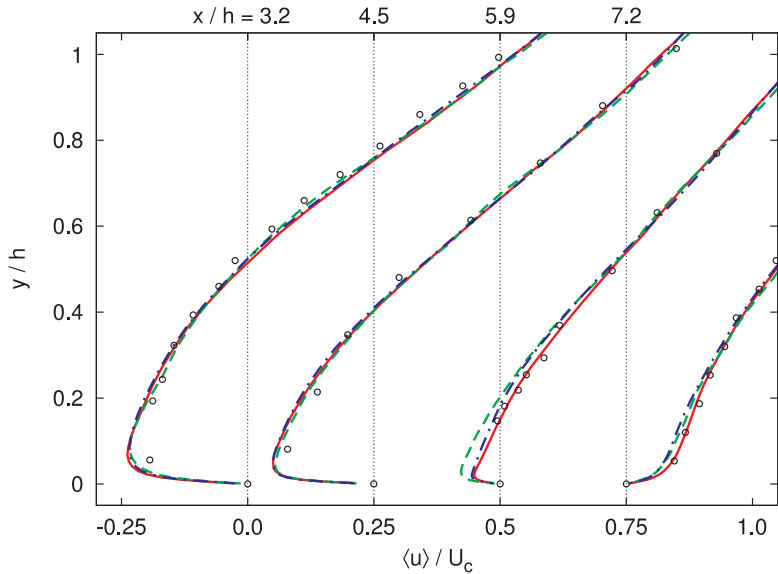


Figure 12. Mean streamwise velocity profiles near the wall: —, LES, dynamic eddy-viscosity model, $144 \times 96 \times 96$; - - -, LES, dynamic eddy-viscosity model, $192 \times 128 \times 128$; - · -, LES, dynamic mixed model, $144 \times 96 \times 96$; ○, Adams *et al* [23].

model generally predicting slightly lower values of the fluctuations. The agreement with the measurements of Vogel and Eaton [1] is reasonable at all locations. At the two locations closest to the step, the LES results deviate from the experiments. It is unclear at this stage why this occurs. Vogel and Eaton [1] attribute the significant scatter in the experimental results near the step to insufficient time averaging [1]. The results obtained on the fine grid also use a shorter sample than the coarse-grid results, and are closer to the experiments. One may conjecture that a combination of these factors, grid resolution in the LES and insufficient sample in the experiments, may be responsible for this difference.

4.5. Turbulent heat fluxes

Streamwise turbulent heat-flux profiles are shown in figure 16. Both subgrid-scale models produce similar results. Two major features are observed in these profiles: a negative peak in the shear layer near the step, and a peak near the wall that is positive near the step, and then changes sign further downstream. The negative peak in the shear layer indicates that in this region, positive streamwise fluctuations associated with fluid moving towards the wall bring cold fluid from above the shear layer down, to mix with the hot fluid underneath. The increase in streamwise heat flux downstream of reattachment is an indication of an increase in the similarity between the temperature and streamwise velocity fields as the flow redevelops. Grid refinement has the effect of moving the near-wall peak of $\langle Tu \rangle$ towards the centre of the recirculation zone. This is the cause of the change in the profiles of temperature fluctuations near the step observed in the previous section. Why this occurs is not clear. No measurements of the streamwise turbulent heat flux are available for comparison; however the present LES results show similar trends to the LES results of Avancha and Pletcher [7] which were obtained at a much lower Reynolds number.

LES of heat transfer downstream of a BFS

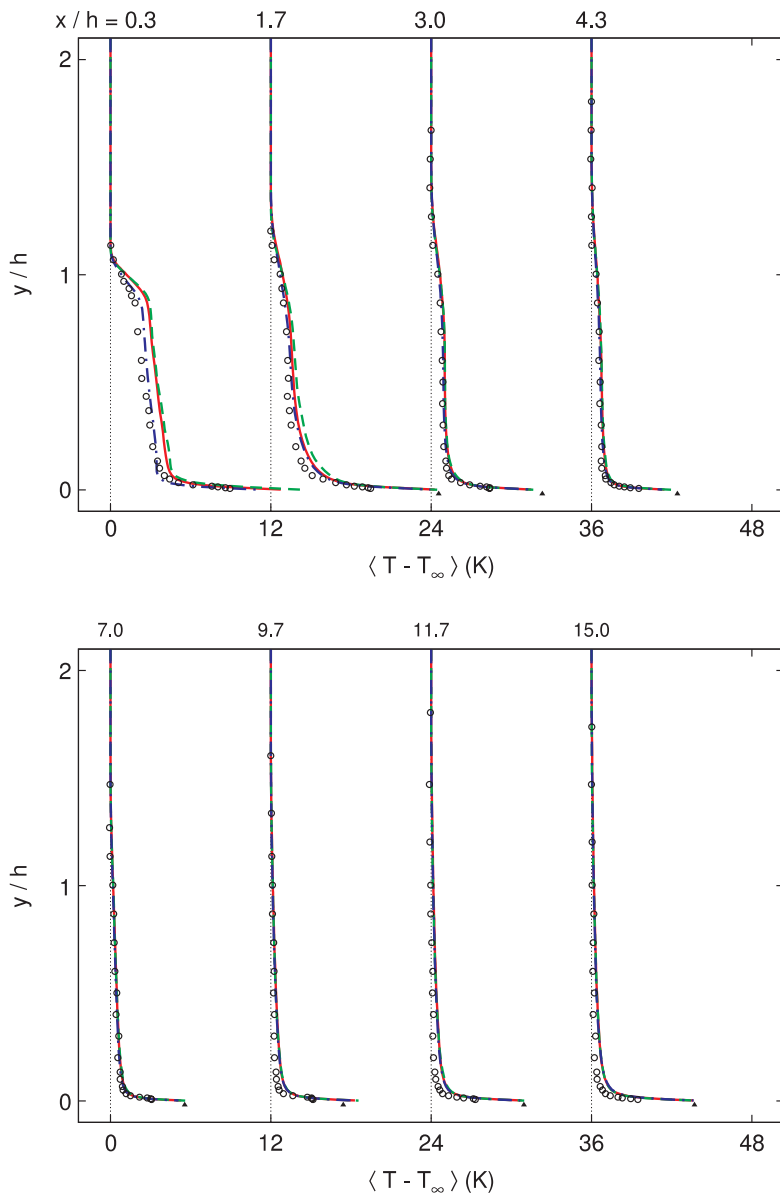


Figure 13. Mean temperature profiles: —, LES, dynamic eddy-viscosity model, $144 \times 96 \times 96$; - - -, LES, dynamic eddy-viscosity model, $192 \times 128 \times 128$; - · -, LES, dynamic mixed model, $144 \times 96 \times 96$; ○, Vogel and Eaton [1].

Profiles of wall-normal turbulent heat flux are shown in figure 17. Differences between the two subgrid-scale models are small (the dynamic mixed model results show a slightly smaller magnitude than the dynamic eddy-viscosity model). These profiles show peaks in the wall-normal turbulent heat flux in the shear layer and near the wall, which indicate that transport across the shear layer and from the wall is driven by positive wall-normal velocity fluctuations. Vogel [22] provides a set of experimental data for the wall-normal turbulent heat flux at a lower Reynolds number, $Re_h = 13\,000$. The present LES results show good qualitative agreement with these experimental results as well as the LES results of Avancha and Pletcher [7]. Grid refinement has little effect on this quantity.

LES of heat transfer downstream of a BFS

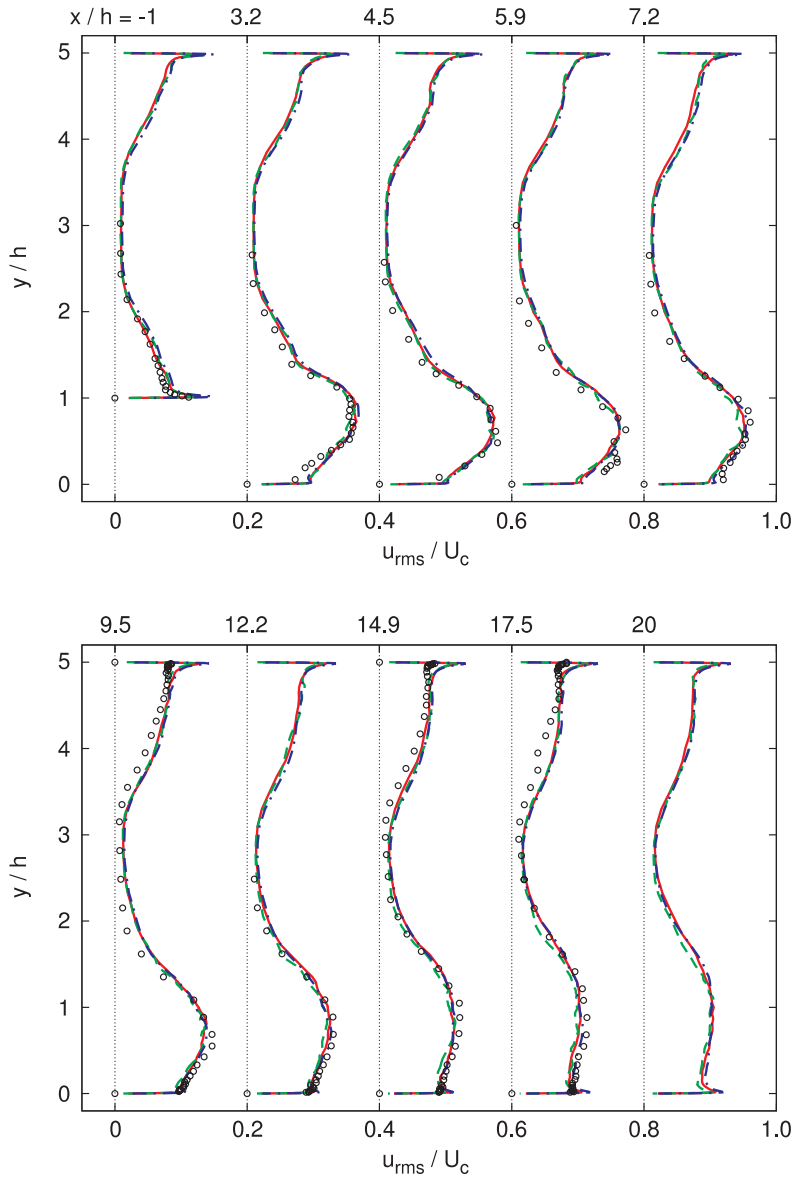


Figure 14. Rms of resolved streamwise velocity fluctuations: —, LES, dynamic eddy-viscosity model, $144 \times 96 \times 96$; - - -, LES, dynamic eddy-viscosity model, $192 \times 128 \times 128$; - · -, LES, dynamic mixed model, $144 \times 96 \times 96$; ○, Adams *et al* [23].

4.6. Mechanisms driving heat transfer in the recirculation zone

As previously discussed, the Reynolds analogy for energy and momentum transport (i.e. $St \propto C_f$) does not hold in the recirculation region. However, the experiments of Vogel and Eaton [1], the LES of Avancha and Pletcher [7] and the present simulations indicate that the heat-transfer rate shows good correlation with the streamwise coefficient-of-friction fluctuations. We also find a direct correlation with the spanwise coefficient-of-friction fluctuations, which were not examined by previous investigators. This correlation seems to be more important downstream of reattachment, where the decay in the spanwise fluctuations (which occurs faster

LES of heat transfer downstream of a BFS

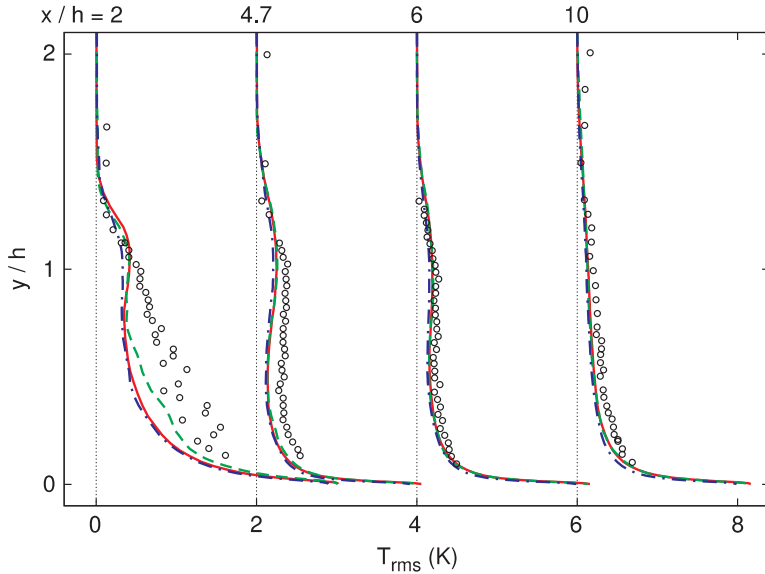


Figure 15. Rms of resolved temperature variance: —, LES, dynamic eddy-viscosity model, $144 \times 96 \times 96$; - - -, LES, dynamic eddy-viscosity model, $192 \times 128 \times 128$; — · —, LES, dynamic mixed model, $144 \times 96 \times 96$; ○, Vogel and Eaton [1].

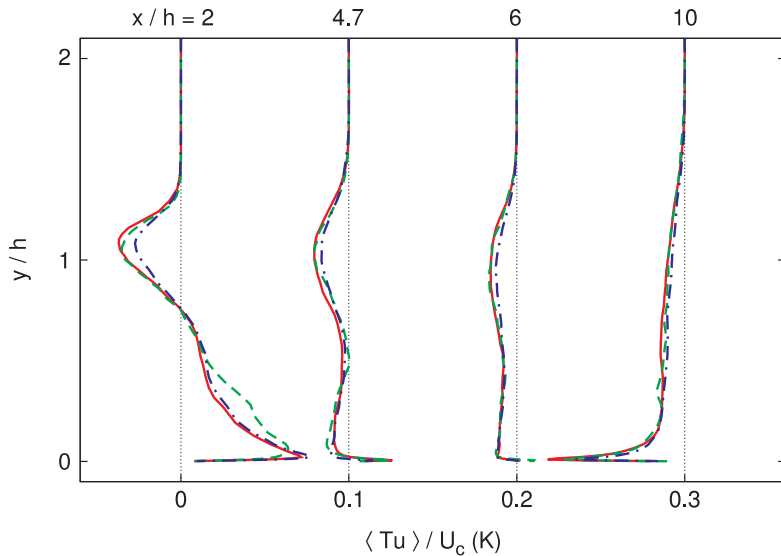


Figure 16. Resolved streamwise turbulent heat flux: —, LES, dynamic eddy-viscosity model, $144 \times 96 \times 96$; - - -, LES, dynamic eddy-viscosity model, $192 \times 128 \times 128$; — · —, LES, dynamic mixed model, $144 \times 96 \times 96$.

than the streamwise fluctuations) better matches the rate-of-decay in the Stanton number profile. As mentioned above, the faster decay of the spanwise fluctuations is caused by the lack of impingement of shear layer eddies downstream of reattachment.

Figures 18 and 19 show scatter plots of fluctuations in wall temperature and streamwise shear stress, and wall temperature and spanwise shear stress respectively. Far downstream of the reattachment point the scatter plot shows the development of a linear correlation as the

LES of heat transfer downstream of a BFS

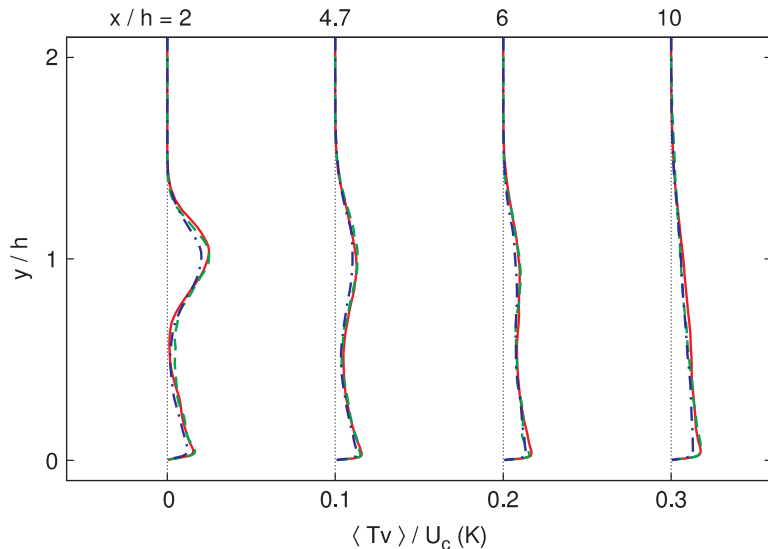


Figure 17. Resolved wall-normal turbulent heat flux: —, LES, dynamic eddy-viscosity model, $144 \times 96 \times 96$; - - -, LES, dynamic eddy-viscosity model, $192 \times 128 \times 128$; — · —, LES, dynamic mixed model, $144 \times 96 \times 96$.

temperature field develops the near-wall streaky structure found in the streamwise velocity field. Near reattachment this similarity does not exist and is replaced by a bell-like correlation, which suggests that cold wall-temperatures are mostly associated with high fluctuations in streamwise shear; however, there are also occasions in which cold wall temperatures occur with small fluctuations in streamwise shear. A similar, bell-like correlation is shown for the spanwise shear at the same locations (figure 19). Far downstream, there is little correlation between the spanwise shear and the wall temperature as the heat transfer mechanism changes from the impinging shear layer eddies to fully developed boundary layer flow.

These bell-like correlations are also observable in the instantaneous fields shown in figures 20 and 21 (which match figures 8 and 9 but includes temperature contours instead of wall-normal velocity contours). Here, cold wall-temperatures can be seen to be somewhat correlated with large shear stress events. However, they seem to be better correlated with one end of the structures which make up these events (rather than the event itself).

Of more interest are the scatter plots of the wall temperature and near-wall, wall-normal velocity (taken as the wall-normal velocity, one computational cell off the wall) shown in figure 22. While far downstream of the reattachment point there is little correlation between the wall temperature and wall-normal velocity, a correlation is observed between the two variables near the mean reattachment location. The correlation is non-linear and reveals the mechanism for large negative fluctuations in the wall temperature. This correlation can also be observed by comparing figures 8 and 20. It appears that high values of near-wall, wall-normal velocity (as previously discussed, these are probably the result of shear-layer eddies impinging on the wall) bring cold fluid from above the shear layer towards the wall, cooling the wall, thereby increasing the heat transfer. Figure 21 (which matches figure 9) shows such an event.

5. Conclusions

A large-eddy simulation of heat transfer downstream of a backward-facing step has been performed. Two subgrid-scale models, the dynamic eddy-viscosity, eddy-diffusivity model and

LES of heat transfer downstream of a BFS

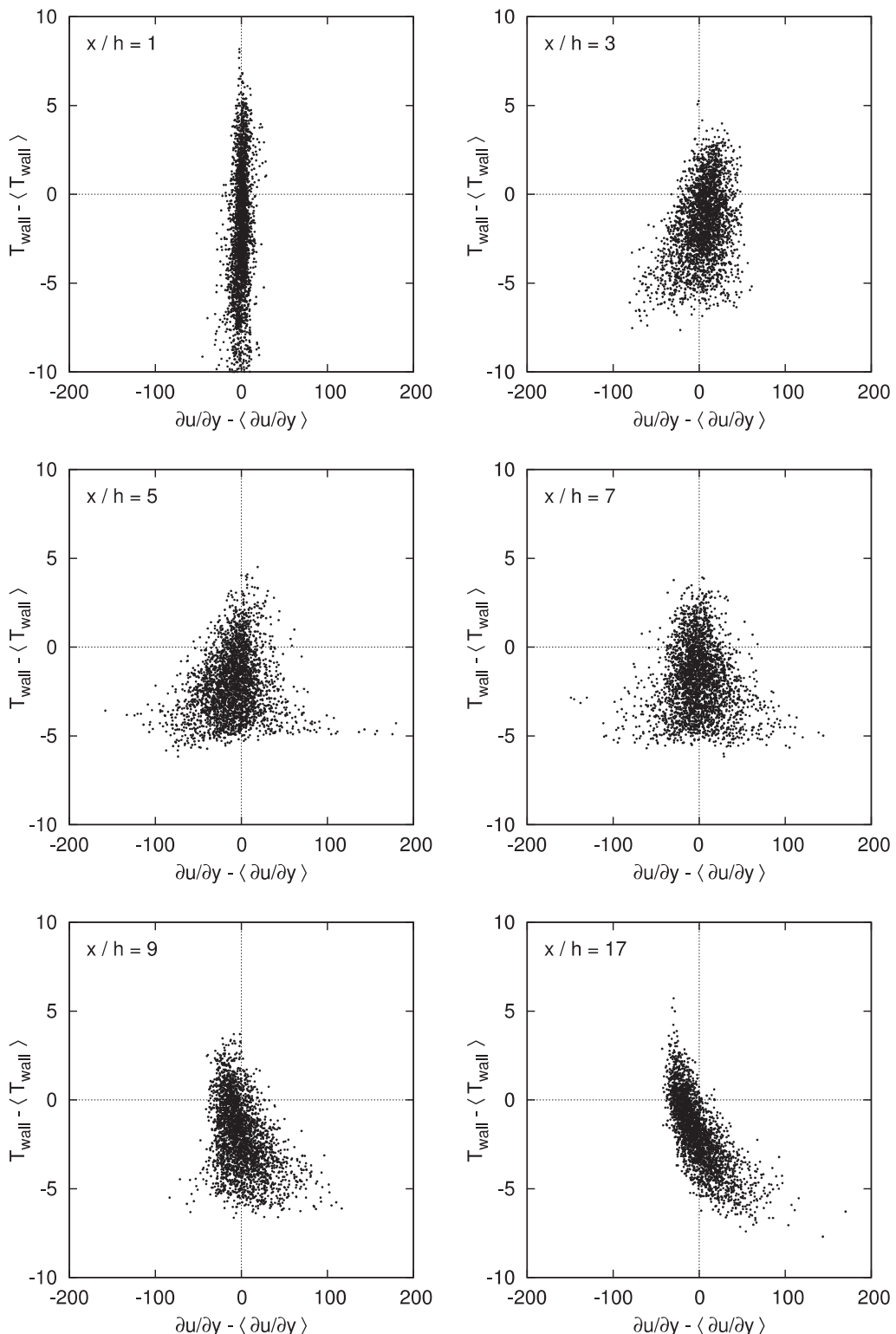


Figure 18. Scatter plots of instantaneous wall temperature and streamwise shear stress.

LES of heat transfer downstream of a BFS

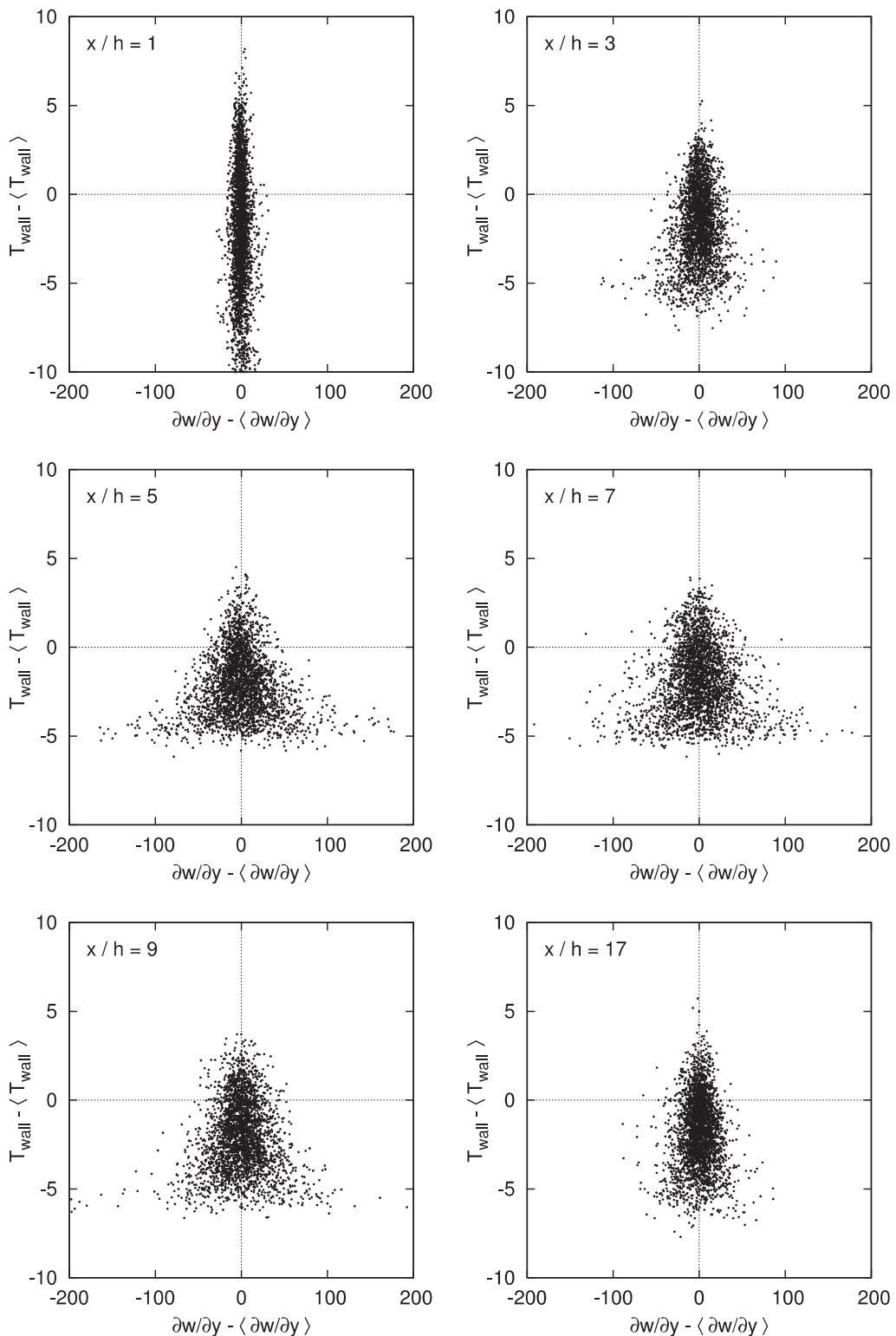


Figure 19. Scatter plots of instantaneous wall temperature and spanwise shear stress.

LES of heat transfer downstream of a BFS

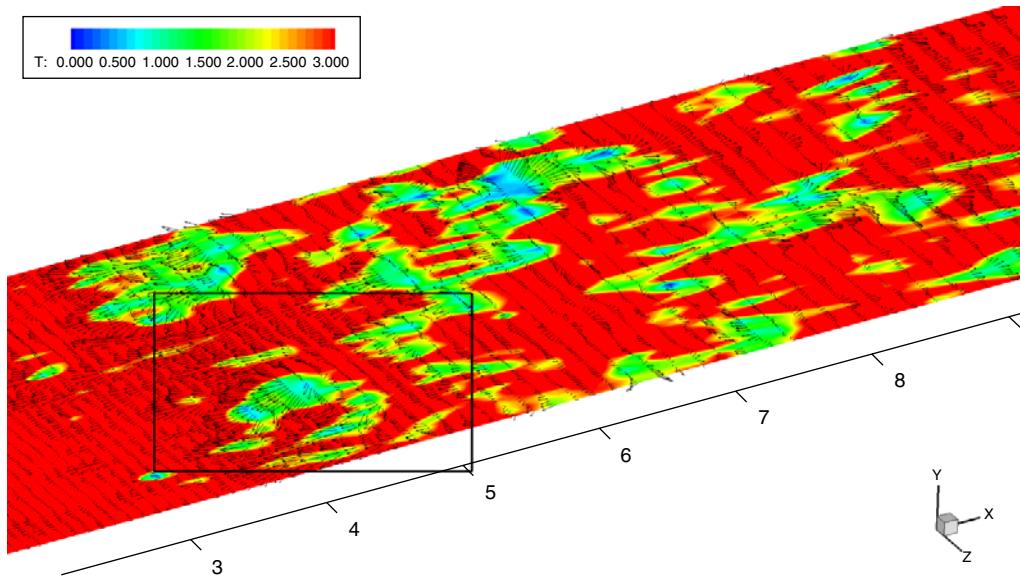


Figure 20. Visualization of wall temperature and wall shear stress vectors. Box indicates extent of figure 21.

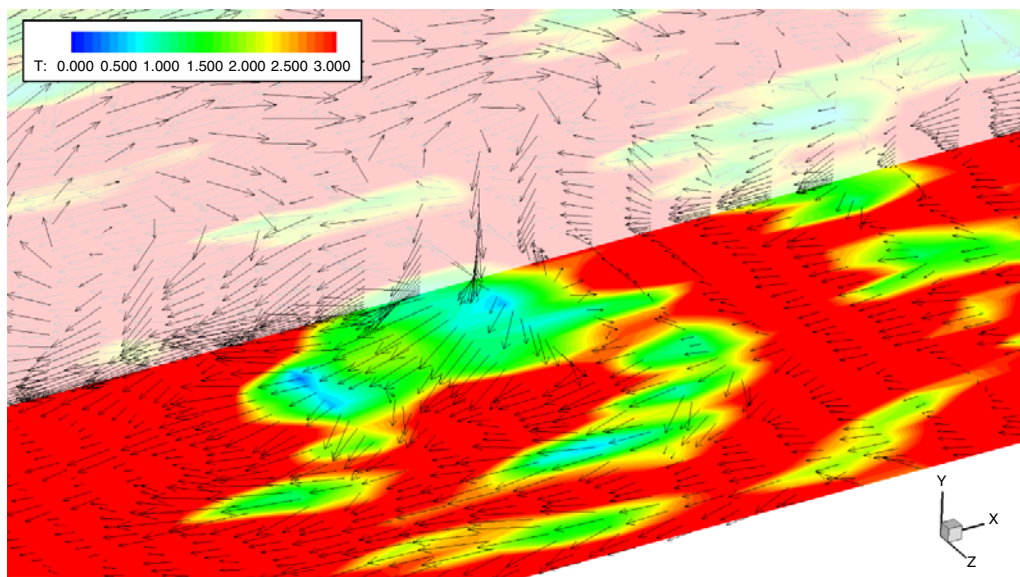


Figure 21. Visualization of a typical ‘downwash’ event. On the xz -horizontal plane are plotted contours of wall temperature with tangential velocity vectors. On the vertical xy -plane (transparent) are tangential velocity vectors.

the dynamic mixed model were tested. Mean reattachment lengths were well predicted by the simulations, errors for both subgrid-scale models were less than 3%. Coefficient of friction predictions were similar to those predicted by the LES of Akselvoll and Moin [19]. Two main discrepancies were found: far downstream of reattachment, the coefficient of friction was underpredicted because of the coarse grid used; and in the recirculation zone the coefficient of friction was overpredicted. It is still unclear why the coefficient of friction is overpredicted in

LES of heat transfer downstream of a BFS

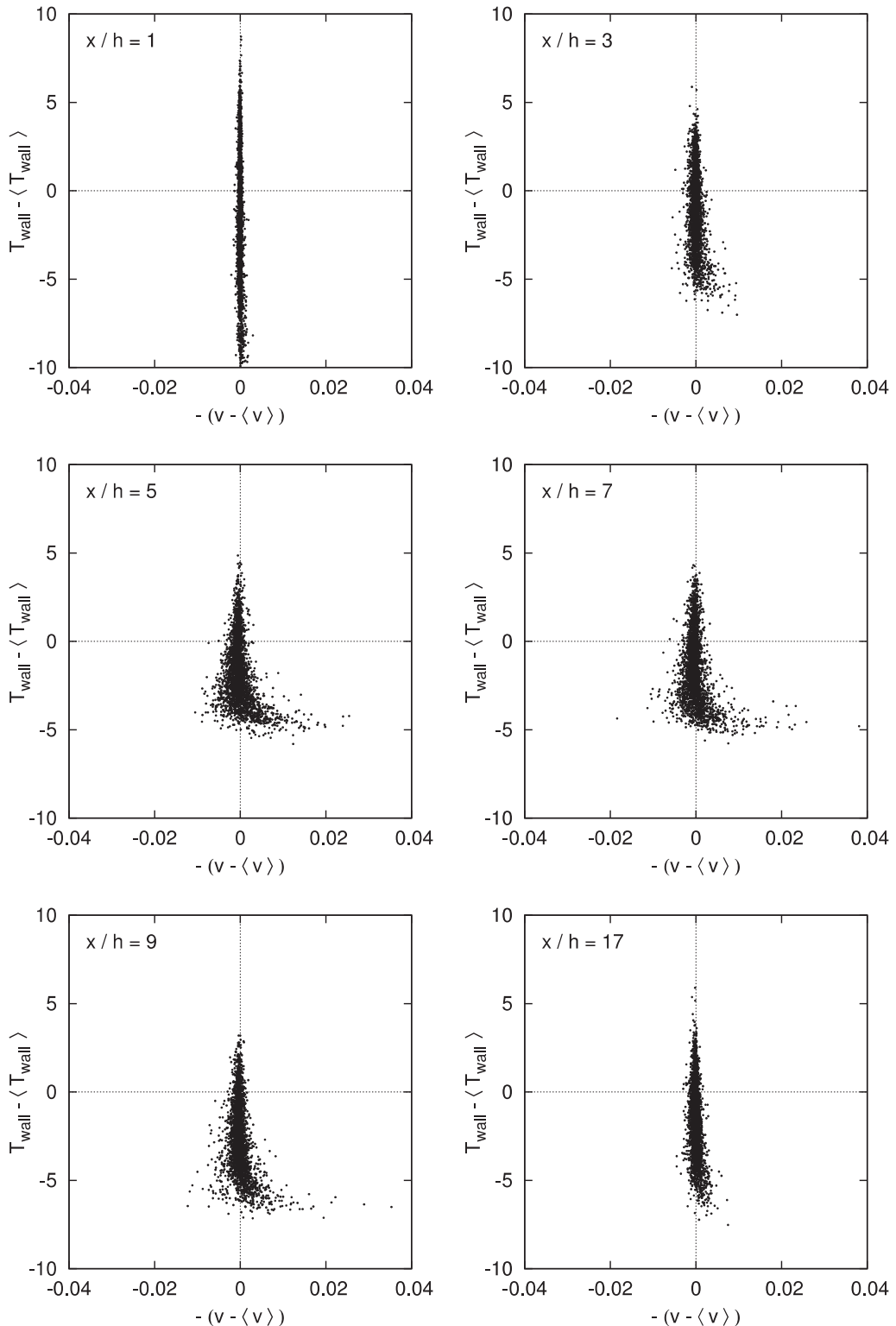


Figure 22. Scatter plots of instantaneous wall temperature and near-wall, wall-normal velocity.

the recirculation zone. Both models produced mean velocity and temperature fields in good agreement with the experimental results of Vogel and Eaton [1]. Predictions of the streamwise velocity fluctuations showed good agreement with the experiments; however there were some differences between the experiments and simulations for the temperature fluctuations near the step edge. Overall, there were few differences between the subgrid-scale model predictions for the velocity field, while dynamic mixed model showed slightly better agreement near the step edge for the temperature field. We also verified grid convergence of the results.

The present simulations confirm the findings by Vogel and Eaton [1] and Avancha and Pletcher [7] in that the peak in heat transfer occurs just upstream of the time-averaged mean reattachment location. An excellent correlation was observed between the heat transfer rate and the streamwise coefficient of friction fluctuations which was also in good agreement with the findings of Vogel and Eaton [1] and Avancha and Pletcher [7].

The simulation results have been analysed with the intent of discovering the mechanism that causes the maximum heat-transfer coefficient to occur upstream of the reattachment point. The peak in the heat-transfer coefficient showed excellent agreement with the peak in the wall shear-stress fluctuations, a fact previously found experimentally [1] and numerically [7]. These shear stress fluctuations were found to be large, and significantly different from those observed in turbulent channel flow. It is proposed that these high levels of shear stress fluctuations are caused by eddies that originate in the shear layer, which later impact the wall. These eddies impact the wall upstream of the reattachment simply because of their size [21] and the associated high momentum. They bring with them cold fluid from above the shear layer and cause a ‘downwash’ of cold fluid when they impact the wall. This mechanism cools the wall, thereby increasing the local level of heat transfer.

Acknowledgments

This work was partially supported by an award under the Merit Allocation Scheme on the National Facility of the Australian Partnership for Advanced Computing.

References

- [1] Vogel J C and Eaton J K 1985 Combined heat transfer and fluid dynamic measurements downstream of a backward facing step *J. Heat Transfer* **107** 922–9
- [2] Abrous A and Emery A F 1996 Benchmark computational results for turbulent backward facing step flow with heat transfer *HTD-Vol 331, ASME National Heat Transfer Conf.* vol 9
- [3] Fletcher L S, Briggs D G and Page R H 1974 Heat transfer in separated and reattached flow: an annotated review *Israel J. Technol.* **12** 236–61
- [4] Aung W and Watkins C 1978 Heat transfer mechanisms in separated forced convection *Proc. NATO Institute on Turbulent Forced Convection in Channel and Bundles: Theory and Applications to Heat Exchangers (Turkey, 20 July–2 August)*
- [5] Aung W 1983 Separated forced convection *ASME/JSME Thermal Engineering Conf. (Honolulu, HI)*
- [6] Kottke V 1984 Heat, mass and momentum transfer in separated flows *Int. J. Chem. Eng.* **24** 86–94
- [7] Avancha R V R and Pletcher R H 2002 Large eddy simulation of turbulent flow past a backward-facing step with heat transfer and property variations *Int. J. Heat Fluid Flow* **23** 601–14
- [8] Labbe O, Sagaut P and Montreuil E 2002 Large-eddy simulation of heat transfer over a backward-facing step *Numerical Heat Transfer A* **42** 73–90
- [9] Kasagi N and Matsunaga A 1995 Three-dimensional particle-tracking velocimetry measurement of turbulence statistics and energy budget in a backward-facing step flow *Int. J. Heat Fluid Flow* **16** 477–85
- [10] Germano M, Piomelli U, Moin P and Cabot W H 1991 A dynamic subgrid-scale eddy viscosity model *Phys. Fluids A* **3** 1760–5

LES of heat transfer downstream of a BFS

- [11] Meneveau C, Lund T S and Cabot W H 1996 A Lagrangian dynamic subgrid-scale model of turbulence *J. Fluid Mech.* **319** 353–85
- [12] Vreman B, Geurts B and Kuerten H 1994 On the formulation of the dynamic mixed subgrid-scale model *Phys. Fluids* **6** 4057–9
- [13] Akselvoll K 1995 Large eddy simulation of turbulent confined coannular jets and turbulent flow over a backward facing step *PhD Thesis* Stanford University
- [14] Leonard B P 1979 A stable and accurate convective modelling procedure based on quadratic upstream interpolation *Comput. Methods Appl. Mech. Eng.* **19** 59–78
- [15] Mittal R and Moin P 1997 Suitability of upwind-biased finite difference schemes for large-eddy simulation of turbulent flows *AIAA J.* **35** 1415–7
- [16] Pierce C D and Moin P 1998 Method for generating equilibrium swirling inflow conditions *AIAA J.* **36** 1325–7
- [17] Kim J and Moin P 1985 Application of a fractional-step method to incompressible Navier–Stokes equations *J. Comput. Phys.* **59** 308–23
- [18] Orlanski I 1976 A simple boundary condition for unbounded hyperbolic flows *J. Comput. Phys.* **21** 252–69
- [19] Akselvoll K and Moin P 1995 Large eddy simulation of turbulent confined coannular jets and turbulent flow over a backward facing step *Technical Report TF-63* Department of Mechanical Engineering, Stanford University
- [20] Jeon S, Choi H, Yoo J Y and Moin P 1999 Space–time characteristics of the wall shear stress fluctuations in a low Reynolds number flow *Phys. Fluids* **11** 3084–94
- [21] Kostas J 2002 An experimental investigation of the structure of a turbulent backward facing step flow *PhD Thesis* Monash University, Victoria
- [22] Vogel J C 1984 Heat transfer and fluid mechanics measurements in the turbulent reattaching flow behind a backward-facing step *PhD Thesis* Stanford University
- [23] Adams E W, Johnston J P and Eaton J K 1984 Experiments on the structure of turbulent reattaching flow *Technical Report MD-43* Thermosciences Division, Department of Mechanical Engineering, Stanford University